ISSN 0965-5425, Computational Mathematics and Mathematical Physics, 2011, Vol. 51, No. 1, pp. 160–173. © Pleiades Publishing, Ltd., 2011.
Original Russian Text © O.V. Bulatov, T.G. Elizarova, 2011, published in Zhurnal Vychislitel'noi Matematiki i Matematicheskoi Fiziki, 2011, Vol. 51, No. 1, pp. 170–184.

Dedicated to Academician A.A. Dorodnicyn on the Occasion of the Centenary of His Birth

Regularized Shallow Water Equations and an Efficient Method for Numerical Simulation of Shallow Water Flows

O. V. Bulatov[a] and T. G. Elizarova[a, b]

[a] *Faculty of Physics, Moscow State University, Moscow, 119992 Russia*

[b] *Institute for Applied Mathematics, Russian Academy of Sciences, Miusskaya pl. 4, Moscow, 125047 Russia*

e-mail: dombulatov@mail.ru, telizar@mail.ru

Received July 25, 2010

Abstract—Regularized shallow water equations are derived as based on a regularization of the Navier–Stokes equations in the form of quasi-gasdynamic and quasi-hydrodynamic equations. Efficient finite-difference algorithms based on the regularized shallow water equations are proposed for the numerical simulation of shallow water flows. The capabilities of the model are examined by computing a test Riemann problem, the flow over an obstacle, and asymmetric dam break.

DOI: 10.1134/S0965542511010052

Keywords: quasi-gasdynamic and quasi-hydrodynamic equations, regularized shallow water equations, finite volume method.

1. INTRODUCTION

The shallow water (SW) equations are a simplified model of the full Navier–Stokes equations, which describe unsteady viscous compressible flows in three dimensions. In the derivation of the SW equations, it is assumed that the medium is a fairly thin layer with a depth much smaller than its horizontal size. Therefore, the vertical velocity in the layer can be neglected, assuming that the horizontal velocities are constant over the depth. Additionally, the fluid is assumed to be incompressible and subject to gravity and its temperature is a constant.

The SW equations are a widely known approximation that underlies the numerical simulation of a variety of problems in ecology, water flows in rivers, reservoirs, and coastal regions in seas and oceans, glacier movements, tsunamis, and atmospheric circulation problems. These problems are closely related to the subject of A.A. Dorodnicyn's earlier works dealing with the motion of air over mountains. Some of the analytical solutions obtained by Dorodnicyn can now be supplemented with numerical solutions of these problems based on the SW equations with allowance for bed roughness.

In the case of no external forces or additional complicating factors, the SW equations can be derived from the classical Euler equations in the barotropic approximation. This analogy between the SW and Euler equations for an inviscid compressible gas is well known, and that is why numerical algorithms for solving the SW equations are based, as a rule, on methods developed for the Euler equations. This idea is used below. Specifically, previously developed methods for computing three-dimensional unsteady gasdynamic flows are used to construct algorithms for flow computation in the shallow water approximation.

In [1–4] a method for regularizing the Navier–Stokes and Euler equations was proposed and studied, which makes it possible to construct efficient numerical algorithms. These algorithms are based on the quasi-gasdynamic (QGD) and quasi-hydrodynamic (QHD) equations, which have been successfully used in the numerical simulation of a wide variety of compressible and incompressible viscous flows. In contrast to the Navier–Stokes and Euler equations, the QGD/QHD equations have additional conservative terms appearing due to the introduction of a two-velocity gasdynamic flow model, which is caused by selecting diffusive fluxes in the continuity equation. The additional terms play the role of regularizers and ensure the stability and accuracy of numerical algorithms constructed with allowance for these terms. Specifically, for the QGD/QHD equations, a theorem is proved stating that the total thermodynamic entropy does not decrease, which confirms the dissipative character of the additional terms.

In this paper, we describe two methods for constructing regularized SW equations and show that they are directly related to the QGD/QHD equations. The first method is based on the barotropic approximation of the QGD/QHD equations, while the second method uses an integral representation of the original SW equations and allows one to obtain the corresponding additional terms to various versions of these

equations. Finite-difference algorithms for the SW equations are proposed, which are closely related to existing methods for solving the QGD/QHD equations. As examples, we solve the Riemann problem and compute the flow over an obstacle and asymmetric dam break in two dimensions.

2. SHALLOW WATER EQUATIONS AS THE BAROTROPIC APPROXIMATION OF THE GASDYNAMIC EQUATIONS

In some works (see, e.g., [5–8]), an analogy is drawn between the SW equations and the Euler equations describing inviscid gasdynamic flows.

In the flux representation, the Euler equations are written as

$$\frac{\partial \rho}{\partial t} + \operatorname{div} \rho \mathbf{u} = 0, \tag{1}$$

$$\frac{\partial (\rho \mathbf{u})}{\partial t} + \operatorname{div}(\rho \mathbf{u} \otimes \mathbf{u}) + \nabla p = 0, \tag{2}$$

$$\frac{\partial E}{\partial t} + \operatorname{div}[\mathbf{u}(E + p)] = 0. \tag{3}$$

Here, the unknowns are the gas density $\rho(\mathbf{x}, t)$, the velocity $\mathbf{u}(\mathbf{x}, t)$, and the total specific energy E. For an ideal polytropic gas, $E = \rho(\mathbf{u}^2/2 + \varepsilon) = 0.5\rho\mathbf{u}^2 + p/(\gamma - 1)$. Here, $p(\mathbf{x}, t)$ and $\varepsilon(\mathbf{x}, t)$ are the pressure and internal energy of the gas, which are related via the equation of state, and γ is the ratio of specific heats.

The barotropic approximation of the gasdynamic equations is a simplification in which the pressure in the gas is assumed to depend only on density:

$$p = p(\rho). \tag{4}$$

Then the total energy equation is eliminated from the general system, and the concept of the first adiabatic index is introduced:

$$\Gamma(\rho) = \frac{\rho p'(\rho)}{p(\rho)}; \tag{5}$$

for an ideal polytropic gas, $\Gamma = \gamma$.

Using the barotropic approximation of system (1)–(3) for a two-dimensional plane flow and setting

$$\rho = h, \quad p(h) = gh^2/2 \quad \text{and} \quad \Gamma = 2, \tag{6}$$

we derive the SW equations for flows over a flat bed (see, e.g., [8]). Here, g is the acceleration due to gravity. Thus, for flat-bed flows in the case of no external forces, the SW equations have the form

$$\frac{\partial h}{\partial t} + \operatorname{div} h\mathbf{u} = 0, \tag{7}$$

$$\frac{\partial (h\mathbf{u})}{\partial t} + \operatorname{div}(h\mathbf{u} \otimes \mathbf{u}) + \nabla \frac{gh^2}{2} = 0. \tag{8}$$

Here, the unknowns are the fluid height (depth) $h(\mathbf{x}, t)$ and the fluid velocity $\mathbf{u}(\mathbf{x}, t)$.

In the SW model, the analogue of the Mach number in gas dynamics, $\mathrm{Ma} = \sqrt{\mathbf{u}^2}/c$, where $c = \sqrt{\gamma RT}$ is the speed of sound in the gas, is the Froude number $\mathrm{Fr} = \sqrt{\mathbf{u}^2}/c$. Moreover, the velocity of propagation of small perturbations is calculated as $c = \sqrt{gh}$.

In [1–3], two systems of equations were derived that extend the Navier–Stokes equations; they are called the systems of quasi-gasdynamic (QGD) and quasi-hydrodynamic (QHD) equations. Both systems can be viewed as the Euler or Navier–Stokes equations with regularizers, which allow one to construct efficient numerical methods for a wide range of problems in gas dynamics. In the barotropic approximation, the QGD and QHD equations can be used to derive two versions of regularized SW equations for flat-bed flows, respectively.

In the traditional notation, the QGD/QHD equations with zero external forces and sources have the form

$$\frac{\partial \rho}{\partial t} + \operatorname{div}\mathbf{j}_m = 0, \tag{9}$$

$$\frac{\partial(\rho\mathbf{u})}{\partial t} + \operatorname{div}(\mathbf{j}_m \otimes \mathbf{u}) + \nabla p = \operatorname{div}\Pi, \tag{10}$$

$$\frac{\partial E}{\partial t} + \operatorname{div}\left[\frac{\mathbf{j}_m}{\rho}(E+p)\right] + \operatorname{div}\mathbf{q} = \operatorname{div}(\Pi \cdot \mathbf{u}). \tag{11}$$

In contrast to the Navier–Stokes equations, the mass flux density $\mathbf{j}_m$ is not equal to the momentum flux $\rho\mathbf{u}$ but differs from the latter by a small quantity $\mathbf{w}$:

$$\mathbf{j}_m = \rho(\mathbf{u} - \mathbf{w}). \tag{12}$$

Thus, the QGD/QHD systems are two-velocity models, i.e., systems of equations involving the velocity $\mathbf{j}_m/\rho$, which is related to the mass flux, and the velocity $\mathbf{u}$, which is related to the momentum flux. These velocities differ by a small quantity $\mathbf{w}$. As a result, a small additional term appears in the viscous stress tensor and the heat flux.

For the QHD system of equations derived by Yu.V. Sheretov in 1996, the addition to the velocity and the viscous stress tensor are given by the formulas

$$\mathbf{w} = \frac{\tau}{\rho}[\rho(\mathbf{u}\cdot\nabla)\mathbf{u} + \nabla p], \tag{13}$$

$$\Pi = \Pi_{\mathrm{NS}} + \rho\mathbf{u} \otimes \mathbf{w}, \tag{14}$$

where Π_{NS} is the Navier–Stokes viscous stress tensor. For this QHD system, the heat flux coincides with the corresponding quantity $\mathbf{q} = \mathbf{q}_{\mathrm{NS}}$ for the Navier–Stokes equations. Here, τ is a small quantity with the dimension of time, which is called a regularization parameter or a time-smoothing parameter. The terms with the coefficient τ can be regarded as regularizing additional terms in the Navier–Stokes equations.

For the QGD system, the corresponding quantities have a more complex form. They are given by the formulas

$$\mathbf{w} = \frac{\tau}{\rho}[(\operatorname{div}(\rho\mathbf{u} \otimes \mathbf{u}) + \nabla p], \tag{15}$$

$$\Pi = \Pi_{\mathrm{NS}} + \tau\mathbf{u} \otimes [\rho(\mathbf{u}\cdot\nabla)\mathbf{u} + \nabla p] + \tau I[(\mathbf{u}\cdot\nabla)p + \gamma p \operatorname{div}\mathbf{u}], \tag{16}$$

$$\mathbf{q} = \mathbf{q}_{\mathrm{NS}} - \tau\rho\mathbf{u}\left[(\mathbf{u}\cdot\nabla\varepsilon) + p(\mathbf{u}\cdot\nabla)\left(\frac{1}{\rho}\right)\right]. \tag{17}$$

It has been shown that the regularizing terms have a dissipative character and have the order of $O(\tau^2)$ for steady flows. The barotropic approximations of the QGD/QHD equations were studied in [9–11].

By analogy with the classical approach, passing to the barotropic approximation in system (9)–(12) for two-dimensional flows and making substitution (6), we obtain a regularized system of SW equations of the form

$$\frac{\partial h}{\partial t} + \operatorname{div}\mathbf{j}_m = 0, \tag{18}$$

$$\frac{\partial(h\mathbf{u})}{\partial t} + \operatorname{div}(\mathbf{j}_m \otimes \mathbf{u}) + \nabla\frac{gh^2}{2} = \operatorname{div}\Pi, \tag{19}$$

where, as before, the mass flux is denoted by $\mathbf{j}_m$ and is given by the formula

$$\mathbf{j}_m = h(\mathbf{u} - \mathbf{w}). \tag{20}$$

For the QHD system, the additions to the velocity and the viscous stress tensor (13), (14) in the SW approximation are given by the formulas

$$\mathbf{w} = \tau[(\mathbf{u}\cdot\nabla)\mathbf{u}) + g\nabla h], \tag{21}$$

$$\Pi = \Pi_{NS} + h\mathbf{u} \otimes \mathbf{w}. \tag{22}$$

For the QGD system, the corresponding quantities are constructed as based on (15) and (16) and are given by the formulas

$$\mathbf{w} = \frac{\tau}{h}\left[(\mathrm{div}(h\mathbf{u} \otimes \mathbf{u}) + \nabla\frac{gh^2}{2}\right], \tag{23}$$

$$\Pi = \Pi_{NS} + \tau\mathbf{u} \otimes \left[h(\mathbf{u} \cdot \nabla)\mathbf{u} + \nabla\frac{gh^2}{2}\right] + \tau I\left[(\mathbf{u} \cdot \nabla)\frac{gh^2}{2} + gh^2\mathrm{div}\mathbf{u}\right]. \tag{24}$$

Depending on the problem in question, Π_{NS} is included into or dropped from the equations.

Thus, by applying the barotropic approximation (6) to the QGD and QHD equations, we obtain two systems of SW equations with regularizers. Both systems are constructed in the simplest case of flows over a flat bed with no external forces.

In Section 3, we describe a method for constructing regularized SW equations with allowance for bed roughness and external forces. The latter can be, for example, wind, the Coriolis force, or bed friction. The approach described can be used to construct regularizers for other forms of SW equations arising in applications.

3. EXAMPLE OF CONSTRUCTION OF GENERAL REGULARIZED EQUATIONS

In [1, 3] a method for deriving the QHD/QGD equations was proposed based on three basic conservation laws written for a small but finite fixed volume of gas. In [2] this method was used to derive the QGD equations for gas flows with allowance for external forces and heat sources.

This approach is used below to construct regularized SW equations with allowance for external forces and bed roughness. We start from the two-dimensional SW equations written in the flux form (see [8]):

$$\frac{\partial h}{\partial t} + \frac{\partial u_x h}{\partial x} + \frac{\partial u_y h}{\partial y} = 0, \tag{25}$$

$$\frac{\partial hu_x}{\partial t} + \frac{\partial}{\partial x}\left(hu_x^2 + \frac{1}{2}gh^2\right) + \frac{\partial}{\partial y}(hu_xu_y) = hf_x - gh\frac{\partial b}{\partial x}, \tag{26}$$

$$\frac{\partial hu_y}{\partial t} + \frac{\partial}{\partial x}(hu_xu_y) + \frac{\partial}{\partial y}\left(hu_y^2 + \frac{1}{2}gh^2\right) = hf_y - gh\frac{\partial b}{\partial y}. \tag{27}$$

In system (25)–(27), the unknowns are the velocity components $u_x(x, y, t)$ and $u_y(x, y, t)$ and the water height $h(x, y, t)$, which is measured from the bed, whose profile is given by the function $b(x, y)$. Here, f_x and f_y denote the components of the given external force.

Following the method for deriving the QHD/QGD equations from the Navier–Stokes equations, system (25)–(27) is rewritten in an integral form by applying integration over a small but finite volume ΔV with the boundary Σ. The differential time derivative is replaced by its difference analogue computed on the finite time step Δt:

$$\int_V \frac{\hat{h} - h}{\Delta t}dV + \int_\Sigma h^*u_i^*d\sigma = 0, \tag{28}$$

$$\int_V \frac{\hat{h}\hat{u}_i - hu_i}{\Delta t}dV + \int_\Sigma \Lambda_{ij}^*d\sigma = \int_V h^*\left(f_i - g\frac{\partial b}{\partial x_i}\right)dV. \tag{29}$$

Here, for notational convenience, we used the index form of the original system (25)–(27) and introduced the tensor $\Lambda_{i,j}$ with components

$$\Lambda_{xx} = hu_x^2 + \frac{1}{2}gh^2, \quad \Lambda_{xy} = \Lambda_{yx} = hu_xu_y, \quad \Lambda_{yy} = hu_y^2 + \frac{1}{2}gh^2.$$

Next, we make the natural assumption that the starred quantities in the integrals correspond to an intermediate time level $t < t^* < t + \Delta t$; i.e., $h^*(x_i, t) = h(x_i, t^*)$ and $u_i^*(x_i, t) = u_i(x_i, t^*)$. Thus, we assume that the fluid height and velocity vary over the short time interval Δt. These variations are small, and if the derivative exists and is sufficiently smooth, they can be estimated, retaining the first term in the series expansion in time. Assigning t^* to the midpoint of the time interval Δt, $t^* = t + \Delta t/2$, and introducing $\tau = (\Delta t)/2$, we can write

$$h^* = h + \tau\frac{\partial h}{\partial t}, \quad u_i^* = u_i + \tau\frac{\partial u_i}{\partial t}. \tag{30}$$

Using expansions (30) and retaining the terms of the first order of smallness in τ yields

$$h^*u_x^* = \left(h + \tau\frac{\partial h}{\partial t}\right)\left(u_x + \tau\frac{\partial u_x}{\partial t}\right) = hu_x + \tau\frac{\partial(hu_x)}{\partial t} + O(\tau^2) = j_{mx} + O(\tau^2). \tag{31}$$

Here, by analogy with the construction of the QHD/QGD systems, we introduced the mass flux expression

$$j_{mx} = h(u_x - w_x),$$

where

$$w_x = \frac{\tau}{h}\left(\frac{\partial(hu_x^2)}{\partial x} + \frac{\partial(hu_xu_y)}{\partial y} + gh\frac{\partial h}{\partial x} + gh\frac{\partial b}{\partial x} - hf_x\right).$$

The time derivatives in (31) were transformed using Eq. (26).

In the same fashion, we obtain

$$h^*u_y^* = \left(h + \tau\frac{\partial h}{\partial t}\right)\left(u_y + \tau\frac{\partial u_y}{\partial t}\right) = hu_y + \tau\frac{\partial(hu_y)}{\partial t} + O(\tau^2) = j_{my} + O(\tau^2),$$

where

$$j_{my} = h(u_y - w_y),$$

and

$$w_y = \frac{\tau}{h}\left(\frac{\partial(hu_xu_y)}{\partial x} + \frac{\partial(hu_y^2)}{\partial y} + gh\frac{\partial h}{\partial y} + gh\frac{\partial b}{\partial y} - hf_y\right).$$

Expressions for the tensor components Λ_{ij}^* at the intermediate time level are derived in a similar manner:

$$\Lambda_{xx}^* = h^*(u_x^*)^2 + \frac{1}{2}g(h^*)^2 = u_xj_{mx} + \frac{1}{2}gh^2 - \Pi_{xx} + O(\tau^2),$$

$$\Lambda_{xy}^* = h^*u_y^*u_x^* = u_yj_{mx} - \Pi_{xy} + O(\tau^2),$$

$$\Lambda_{yx}^* = h^*u_x^*u_y^* = u_xj_{my} - \Pi_{yx} + O(\tau^2),$$

$$\Lambda_{yy}^* = h^*(u_y^*)^2 + \frac{1}{2}g(h^*)^2 = u_yj_{my} + \frac{1}{2}gh^2 - \Pi_{yy} + O(\tau^2).$$

The expressions for Π_{ij} have the form of first spatial derivatives with the coefficient τ:

$$\Pi_{xx} = \tau hu_x\left(u_x\frac{\partial u_x}{\partial x} + u_y\frac{\partial u_x}{\partial y} + g\frac{\partial h}{\partial x} + g\frac{\partial b}{\partial x} - f_x\right) + \tau gh\left(u_x\frac{\partial h}{\partial x} + u_y\frac{\partial h}{\partial y} + h\frac{\partial u_x}{\partial x} + h\frac{\partial u_y}{\partial y}\right),$$

$$\Pi_{yx} = \tau u_yh\left(u_x\frac{\partial u_x}{\partial x} + u_y\frac{\partial u_x}{\partial y} + g\frac{\partial h}{\partial x} + g\frac{\partial b}{\partial x} - f_x\right),$$

$$\Pi_{xy} = \tau u_x h\left(u_x\frac{\partial u_y}{\partial x} + u_y\frac{\partial u_y}{\partial y} + g\frac{\partial h}{\partial y} + g\frac{\partial b}{\partial y} - f_y\right),$$

$$\Pi_{yy} = \tau h u_y\left(u_y\frac{\partial u_y}{\partial y} + u_x\frac{\partial u_y}{\partial x} + g\frac{\partial h}{\partial y} + g\frac{\partial b}{\partial y} - f_y\right) + \tau g h\left(u_y\frac{\partial h}{\partial y} + u_x\frac{\partial h}{\partial x} + h\frac{\partial u_x}{\partial x} + h\frac{\partial u_y}{\partial y}\right).$$

Returning to the integral form of Eqs. (28) and (29), dropping the terms of order $O(\tau^2)$, and replacing the difference time derivative by its differential analogue, we obtain the differential SW equations

$$\frac{\partial h}{\partial t} + \frac{\partial j_{mx}}{\partial x} + \frac{\partial j_{my}}{\partial y} = 0, \tag{32}$$

$$\frac{\partial h u_x}{\partial t} + \frac{\partial j_{mx}u_x}{\partial x} + \frac{\partial j_{my}u_x}{\partial y} + \frac{\partial}{\partial x}\left(\frac{gh^2}{2}\right) = h^*\left(f_x - g\frac{\partial b}{\partial x}\right) + \frac{\partial \Pi_{xx}}{\partial x} + \frac{\partial \Pi_{yx}}{\partial y}, \tag{33}$$

$$\frac{\partial h u_y}{\partial t} + \frac{\partial j_{mx}u_y}{\partial x} + \frac{\partial j_{my}u_y}{\partial y} + \frac{\partial}{\partial y}\left(\frac{gh^2}{2}\right) = h^*\left(f_y - g\frac{\partial b}{\partial y}\right) + \frac{\partial \Pi_{xy}}{\partial x} + \frac{\partial \Pi_{yy}}{\partial y}, \tag{34}$$

where

$$h^* = h - \tau\left(\frac{\partial h u_x}{\partial x} + \frac{\partial h u_y}{\partial y}\right). \tag{35}$$

System (32)–(35) is closely related to the original SW equations and, at $\tau = 0$, passes into system (25)–(27). The form of the terms with τ is determined by the form of the original equations. Therefore, stationary solutions of the original system (25)–(27) are stationary solutions of system (32)–(35). An example of such solutions is that of the lake at rest problem: for the steady-state problem with $u_x = u_y = 0$ in the absence of external forces ($f_x = f_y = 0$), the SW equations satisfy the hydrostatic balance condition

$$\frac{\partial}{\partial x_i}\left(\frac{gh^2}{2}\right) + gh\frac{\partial b}{\partial x_i} = 0; \tag{36}$$

i.e., in this case, the water level in the lake is horizontal: $h(x, y) + b(x, y) = \text{const}$. The SW equations with additional terms are also satisfied by this solution, which can be checked by substituting it into system (32)–(35).

The above regularized SW equations correspond to system (18)–(20) with closure (23), (24) derived as the barotropic approximation of the QGD system. A numerical algorithm and numerical examples computed using Eqs. (32)–(35) are given in the next section.

Corresponding to closure (21), (22), the regularized SW equations with allowance for bed roughness and external forces are derived in a similar manner under the assumption that the fluid velocity varies, while the fluid height remains unchanged over the shot time interval τ. This means that we have to set $h^* = h$ in (30). For one-dimensional spatial flows, these SW equations and an example of solving the Riemann problem are given in [12].

4. NUMERICAL SIMULATION OF ONE-DIMENSIONAL FLOWS

For one-dimensional plane flows, the regularized SW equations (32)–(35) have the form

$$\frac{\partial h}{\partial t} + \frac{\partial j_m}{\partial x} = 0, \tag{37}$$

$$\frac{\partial h u}{\partial t} + \frac{\partial j_m u}{\partial x} + \frac{\partial}{\partial x}\left(\frac{gh^2}{2}\right) = g\left(h - \tau\frac{\partial h u}{\partial x}\right)\left(f - \frac{\partial b}{\partial x}\right) + \frac{\partial \Pi}{\partial x}, \tag{38}$$

where

$$j_m = h(u - w), \quad w = \frac{\tau}{h}\left(\frac{\partial h u^2}{\partial x} + gh\frac{\partial h}{\partial x} + gh\frac{\partial b}{\partial x} - hf\right), \tag{39}$$

$$\Pi = \tau uh\left(u\frac{\partial u}{\partial x} + g\frac{\partial h}{\partial x} + g\frac{\partial b}{\partial x} - f\right) + \tau gh\left(u\frac{\partial h}{\partial x} + h\frac{\partial u}{\partial x}\right). \quad (40)$$

By analogy with algorithms developed for the QGD equations, the regularized SW equations (37)–(40) are solved using an explicit difference scheme with all the spatial derivatives approximated by central differences. Difference schemes of this type have proved to be highly efficient and accurate as applied to the computation of viscous compressible gas flows (see, e.g., [1–3, 13]).

The values of the desired variables $h(x, t)$ and $u(x, t)$ are determined at spatial grid points i. The values of the variables at the half-integer spatial points $i + 1/2$ are calculated as the arithmetic mean of the values at neighboring points:

$$h_{i+1/2} = 0.5(h_i + h_{i+1}), \quad u_{i+1/2} = 0.5(u_i + u_{i+1}), \quad b_{i+1/2} = 0.5(b_i + b_{i+1}). \quad (41)$$

By using the values at half-integer points, we compute fluxes (39) and (40) at these points:

$$j_{m,i+1/2} = h_{i+1/2}(u_{i+1/2} - w_{i+1/2}), \quad (42)$$

where

$$w_{i+1/2} = \frac{\tau_{i+1/2}}{h_{i+1/2}}\left(\frac{h_{i+1}u_{i+1}^2 - h_iu_i^2}{\Delta x} + gh_{i+1/2}\frac{h_{i+1} - h_i}{\Delta x} + gh_{i+1/2}\frac{b_{i+1} - b_i}{\Delta x} - h_{i+1/2}f_{i+1/2}\right). \quad (43)$$

In the same manner,

$$\begin{aligned}\Pi_{i+1/2} = \tau_{i+1/2}u_{i+1/2}h_{i+1/2}&\left(u_{i+1/2}\frac{u_{i+1} - u_i}{\Delta x} + g\frac{h_{i+1} - h_i}{\Delta x} + g\frac{b_{i+1} - b_i}{\Delta x} - f_{i+1/2}\right)\\ &+ \tau_{i+1/2}gh_{i+1/2}\left(u_{i+1/2}\frac{h_{i+1} - h_i}{\Delta x} + h_{i+1/2}\frac{u_{i+1} - u_i}{\Delta x}\right).\end{aligned} \quad (44)$$

At the next stage of the numerical method, the first SW equation is approximated as

$$\frac{h_i^{k+1} - h_i^k}{\Delta t} + \frac{j_{m,i+1/2} - j_{m,i-1/2}}{\Delta x} = 0, \quad (45)$$

where the index k denotes the current time level and the time step is Δt. All the spatial derivatives are calculated at the time step k.

The flow rate equation (38) is approximated as follows:

$$\begin{aligned}&\frac{h_i^{k+1}u_i^{k+1} - h_i^ku_i^k}{\Delta t} + \frac{j_{m,i+1/2}u_{i+1/2} - j_{m,i-1/2}u_{i-1/2}}{\Delta x}\\ &+ \frac{g}{2}\frac{h_{i+1/2}^2 - h_{i-1/2}^2}{\Delta x} = gh_i^*\left(f_i - \frac{b_{i+1/2} - b_{i-1/2}}{\Delta x}\right) + \frac{\Pi_{i+1/2} - \Pi_{i-1/2}}{\Delta x}.\end{aligned} \quad (46)$$

Here,

$$h_i^* = 0.5(h_{i+1/2} + h_{i-1/2}) - \tau_i\frac{h_{i+1/2}u_{i+1/2} - h_{i-1/2}u_{i-1/2}}{\Delta x}. \quad (47)$$

The above approximation ensures that the algorithm is well balanced. This means that the numerical scheme does not violate the natural condition that, in the absence of external forces, the fluid at rest with the horizontal surface $h(x) + b(x) = \text{const}$ cannot spontaneously start moving over a rough bed; i.e., the condition $u = 0$ is preserved (the lake at rest problem). This property of the difference scheme can be checked by directly substituting the discrete solution $u_i = 0$, $h_i + b_i = \text{const}$ into the system of difference equations (41)–(47) for the steady-state problem. For well-known numerical algorithms, this property is achieved, as a rule, by applying rather complicated constructions (see, e.g., [14, 15]).

The stability of the numerical algorithm is ensured by the terms with τ. Its value is related to the spatial mesh size Δx and is calculated as

$$\tau = \alpha\frac{\Delta x}{c}, \quad c = \sqrt{gh}, \quad (48)$$

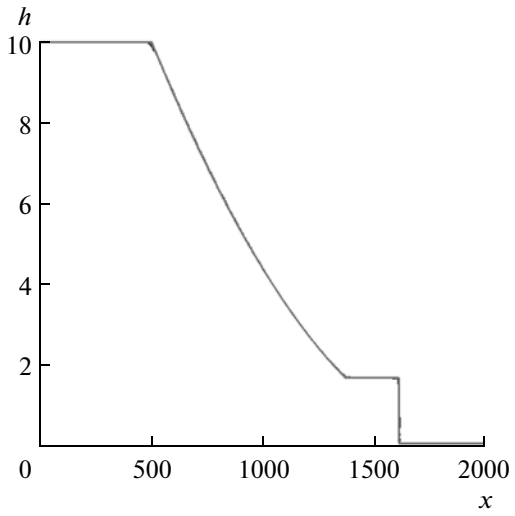

Fig. 1.

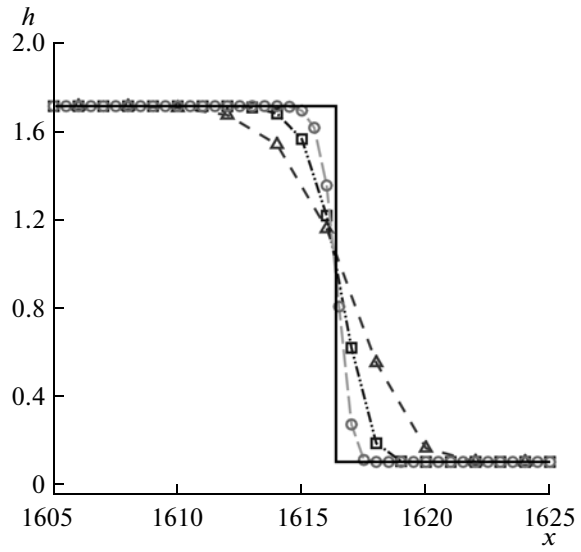

Fig. 2.

where $0 < \alpha < 1$ is a numerical coefficient chosen so as to ensure the accuracy and stability of the algorithm. As a stability condition, we use the Courant condition, where the time step is given by the formula

$$\Delta t = \beta(\Delta x/c)_{\min}. \tag{49}$$

Here, the Courant number β ($0 < \beta < 1$) is a function of τ and is chosen in the course of the computations so as to ensure the stability of the numerical solution.

Below, we present examples of well-known test problems solved using the above-described difference algorithm. Uniform spatial meshes were used in all the computations.

4.1. Test 1: Riemann Problem

The performance of the method was verified by solving the Riemann problem, which is also known as the planar dam break problem. This problem was used in [8, 16] to test numerical difference methods for solving the SW equations based on algorithms based on the first- and second-order accurate Godunov schemes. This problem was also addressed in other publications, for example, in [14], where well-balanced schemes based on the kinetic approach were tested, and in [17], where finite-difference algorithms of an arbitrary order of accuracy were constructed. It was noted in [14] is that most computational algorithms with upwind differences used for flux approximation fail to calculate this test.

Consider the one-dimensional plane flow of a fluid in a channel of length L with a flat bed $b = \text{const}$. Initially, at the center of the domain, there is a discontinuity of the water height separating two homogeneous states with the water heights $h = h_l$ and $h = h_r$ to the left and right of the discontinuity, respectively. Initially, the fluid to the right and left of the discontinuity is at rest: $u_l = u_r = 0$. The Riemann problem was calculated for h_r/h_l ranging from 0.5 to 0.0001, but we present only the results obtained with the same parameters as in [6], where $L = 2000$ m, $h_l = 10$ m, $h_r = 0.1$ m, and $g = 9.8$ m/s^2. The results correspond to $t = 50$ s.

Figure 1 shows the profiles of $h(x)$ computed on a sequence of uniform spatial grids with the mesh sizes $\Delta x = 0.5$, 1, and 2 m (the solid line depicts the self-similar solution). Fragments of the general pattern are presented in Fig. 2, where the grid points are shown by markers: triangles for $\Delta x = 2$ m, squares for $\Delta x = 1$ m, and circles for $\Delta x = 0.5$ m. In the computations, the regularization parameter (48) was calculated at $\alpha = 0.1$. The plots show that the numerical solution converges monotonically to the self-similar one as the spatial grid is refined.

The dependence of the numerical solution on the regularization parameter is demonstrated in Fig. 3 (fragments). Specifically, the figure depicts the profiles of $h(x)$ obtained on a grid with the mesh size $\Delta x = 2$ m for a sequence of regularization parameters (48) calculated at $\alpha = 0.05$, 0.1, 0.2, and 0.3. The time step (49) is $\Delta t = 0.02$ s, which corresponds to the Courant number $\beta = 0.1$. As α increases, the discontinuity of the solution is smoothed. As α decreases, oscillations appear in the numerical solution (at $\alpha = 0.05$) and, with a further decrease in the regularizer, the solution becomes unstable. Experience gained

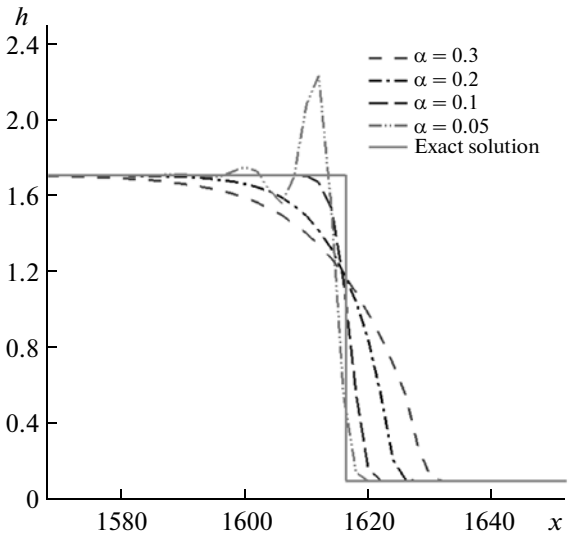

Fig. 3.

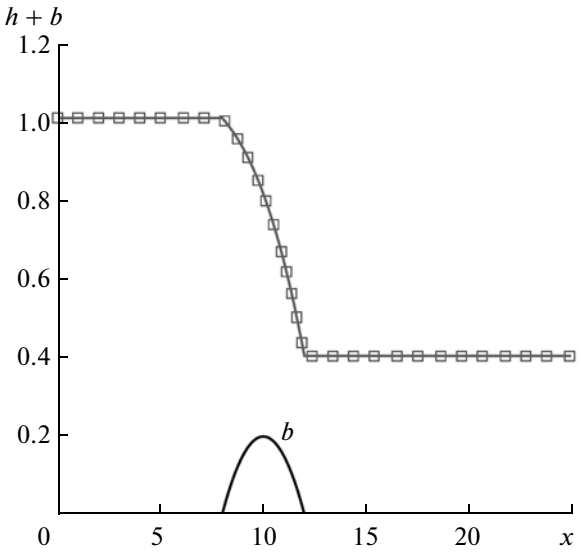

Fig. 4.

from the computations suggests that there are ranges of optimal values of α, Courant number, and the mesh size that ensure the required accuracy of the solution.

For a difference algorithm with a regularizer of form (13), (14), the stability of the discrete solution depending on τ was studied in [12]. It was shown that there is an optimal value of α for which the time step is maximal.

For $\alpha = 0.1$, the discontinuity occupy 5–6 grid points (Fig. 2), and as α decreases, the discontinuity transition can be reduced to 3–5 grid points. In precision numerical algorithms (which are considerably more sophisticated), the discontinuity can be approximated over fewer grid points. In [14], for example, the discontinuity is approximated at 3–4 grid points, while the generalized Riemann method (see [16]) makes it possible to describe the discontinuity over 1–2 grid points. However, these methods are substantially inferior to the authors' algorithm in terms of the amount of arithmetic operations per time step per spatial grid point.

4.2. Test 2: Transcritical Flow over an Obstacle

This test is the classical problem of transcritical flow over an obstacle, where the Froude number varies from smaller-than-unity to large-than-unity values, including supercritical ones. Depending on the initial and boundary conditions, a fixed discontinuity (hydrodynamic jump) may or may not form in the flow. For flows with no discontinuity, the SW equations have the exact solution

$$hu = Q_0 = \text{const}, \quad \frac{Q_0^2}{2gh^2} + h + b = \text{const}_1.$$

The SW equations with a regularizer are also satisfied by this solution, since, for it, all the terms with τ vanish.

Following [14], consider two most complicated case of transcritical flow with and without the formation of a hydrodynamic discontinuity. The length of the channel is 25 m, and the shape of the bed is described by the function $b(x) = 0.2 - 0.05(x - 10)^2$, if $8 < x < 12$, and $b(x) = 0$ otherwise.

Case 1: flow with no discontinuity. The left boundary condition was $hu = 1.53 m^2/s$, $\partial h/\partial x = 0$. The flow drift conditions were set on the right: $\partial h/\partial x = 0$, $\partial u/\partial x = 0$. The initial condition was specified as $h + b = 0.4$ m, $u = 0$.

The computed values of hu and j_m agree to high accuracy with the analytical solution of this problem: $Q_0 = j_m = hu = 1.53$ m^2/s. In the region over the bed hump, the difference between the computed and exact values of hu is ~0.001 m^2/s. The computations were performed for $\alpha = 0.6$, $\beta = 0.05$, and $\Delta x = 0.0625$ and 0.125 m. The last value coincides with that in [14], but the error in the computed value of hu over the bed

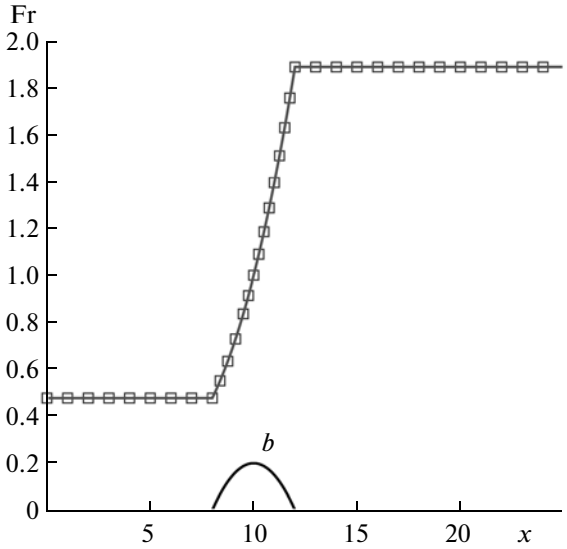

Fig. 5.

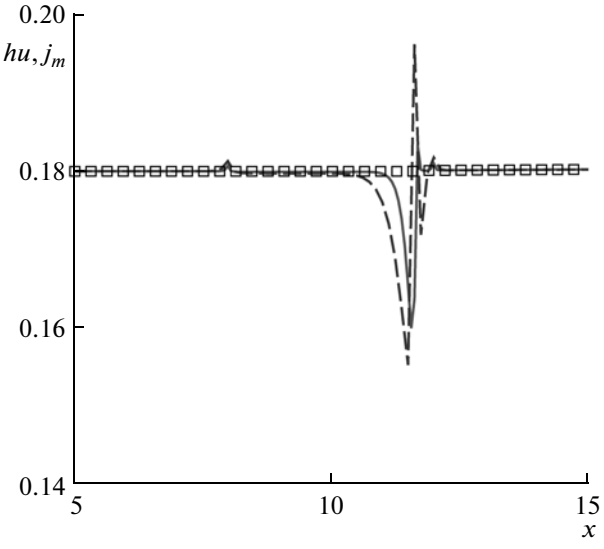

Fig. 6.

hump is less than in that [14], where a cumbersome gas-kinetic algorithm was used. It is well known that the accurate determination of the flow rate over an obstacle is computationally more difficult than finding the fluid velocity or height in this region.

Figures 4 and 5 depict the distribution of $h + b$ and the Froude number for the mesh sizes $\Delta x =$ 0.0625 m (solid line) and 0.125 m (squares). It can be seen that the numerical solutions differ little as the grid is refined, which suggests the achieved accuracy. It can also be seen that the flow is transcritical: while passing over the bed hump, the velocity increases so that the Froude number becomes higher than unity (Fig. 5).

Case 2. Flow with a fixed discontinuity. The formation of a hydrodynamic discontinuity was caused by the following boundary and initial conditions: on the left boundary, we set $hu = 0.18$ m^2/s and $\partial h/\partial x = 0$, while, on the right boundary, $h = 0.33$ m and $\partial u/\partial x = 0$. The initial conditions were specified as $h + b =$ 0.33 m, $u = 0$.

The numerical solution behind the discontinuity exhibited computational instability manifested in grid oscillations of the solution. To smooth these nonphysical oscillations, by analogy with the QGD algorithm for supersonic gas flows, the term

$$\Pi_{\mathrm{NS}} = \tau\frac{gh^2}{2}\frac{\partial u}{\partial x}$$

was added to expression (40) for the viscous stress tensor. This term is an additional regularizer of the type of Navier–Stokes viscosity.

The computations were performed for $\alpha = 0.6$, $\beta = 0.1$, and $\Delta x = 0.125$ m (dashed line) and 0.0625 m (solid line). The results are presented in Figs. 6–8.

Figure 6 depicts the computed values of j_m (squares) and hu. The exact solution of the problem corresponds to the flow rate $Q_0 = hu = 0.18$ m^2/s. In the entire flow region, $j_m = Q_0$ for both grids. The flow rate hu agrees well with the analytical value everywhere, except for a narrow zone near the discontinuity, where oscillations are observed in a domain that occupies 8–10 mesh steps and decreases with mesh refinement.

Figures 7 and 8 show the distribution of the fluid height and the Froude number for the indicated grids. It can be seen that the computed fluid heights are very close for both grids (Fig. 7) and that the numerical results for the Froude number converge monotonically to the analytical solution (Fig. 8). The maximum Froude number is $\mathrm{Fr}_{\max} = 2.35$ for $\Delta x = 0.125$ m and $\mathrm{Fr}_{\max} = 2.48$ for $\Delta x = 0.0625$ m, while the analytical value is $\mathrm{Fr}_{\max} = 2.78$. Note that, in contrast to the results presented in [14] and in the works cited in [14], the Froude number does not become higher than its analytical value.

According to [14], the agreement between the numerical and analytical solutions above the obstacle is the most difficult problem for nearly all numerical algorithms.

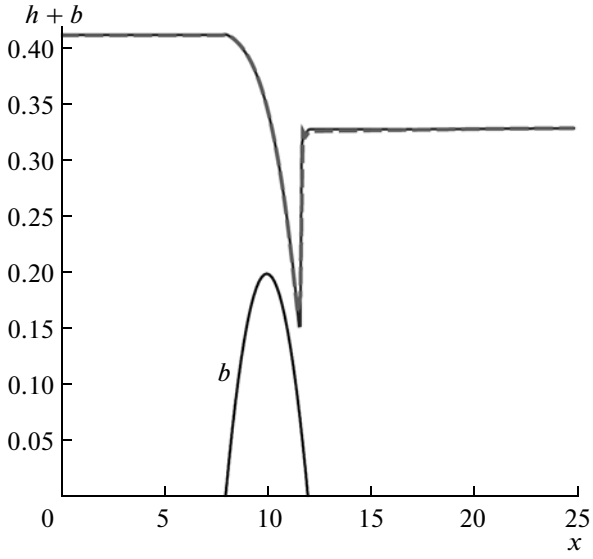

Fig. 7.

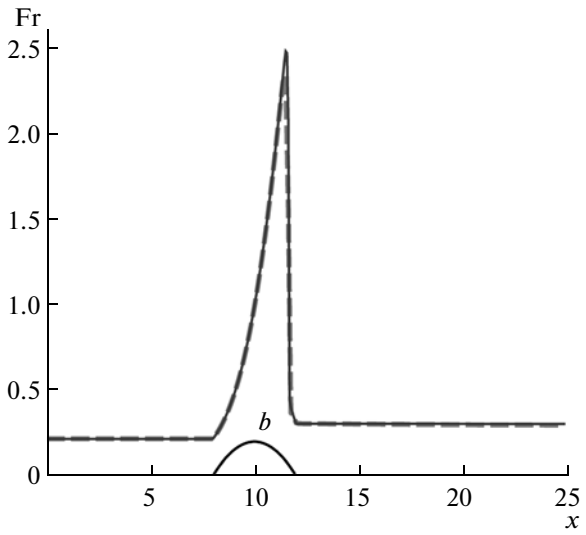

Fig. 8.

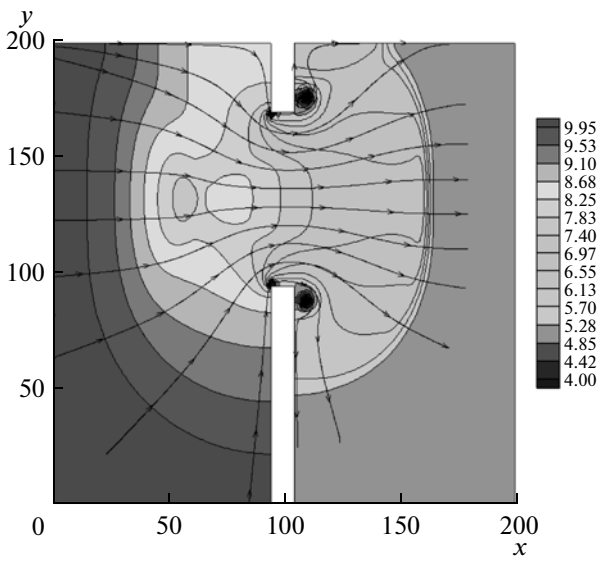

Fig. 9.

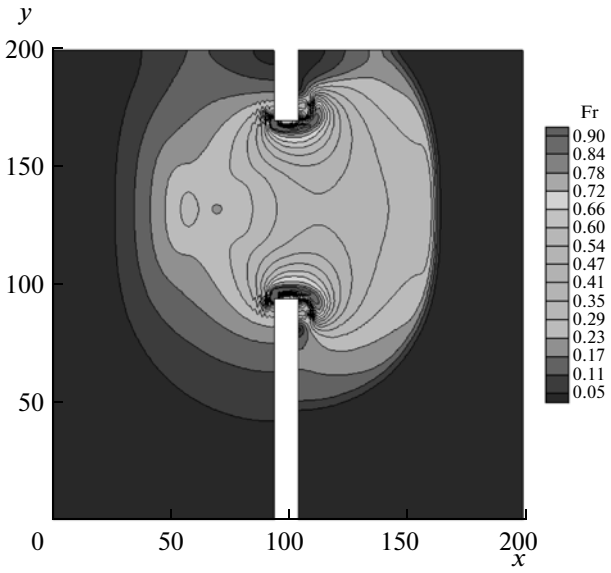

Fig. 10.

5. COMPUTATIONAL SCHEME FOR TWO-DIMENSIONAL FLOWS AND ASYMMETRIC DAM BREAK

A numerical algorithm for two-dimensional flows is constructed in the same manner as for one-dimensional flows. System (32)–(35) is approximated using the finite volume method with all the spatial derivatives approximated by second-order accurate central differences. Overall, the method is similar to that used for solving the QGD equations for two-dimensional flows (see, e.g., [2, 13]).

The capabilities of the two-dimensional algorithm are illustrated by computing the unsteady flow caused by an asymmetric dam break. This is a well-known test problem. Its formulation can be found, for example, in [17, 18] (see also the references therein). In these computations, the external forces are ignored ($f_x = f_y = 0$) and the bed is assumed to be flat: $b(x, y) = 0$.

Following [18], we considered the flow generated by an instantaneous break of a dam separating two water basins. The water heights in the left and right basins were 10 and 5 m, respectively. The length of the discontinuity was 75 m, and the beginning of the discontinuity was located at the point with coordinate $y = 95$ m (see Fig. 9). The thickness of the dam wall was 10 m, and its left-hand side was located at the

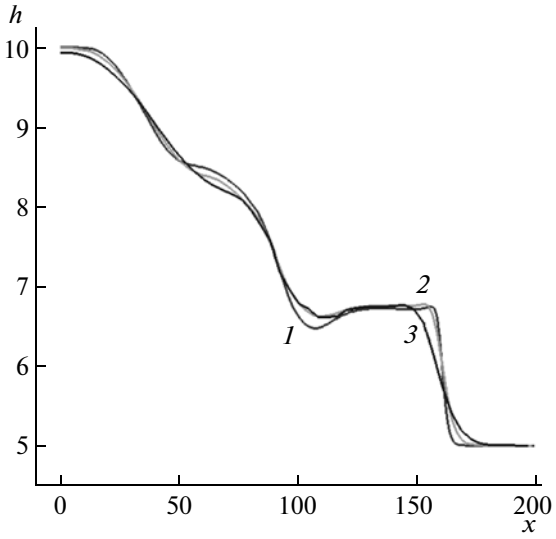

Fig. 11.

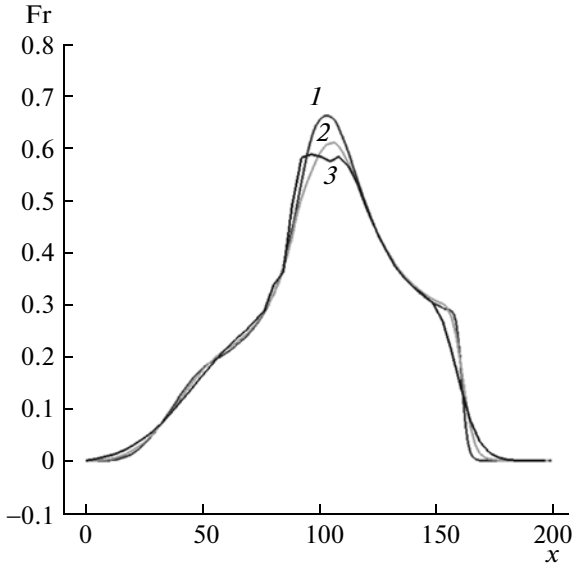

Fig. 12.

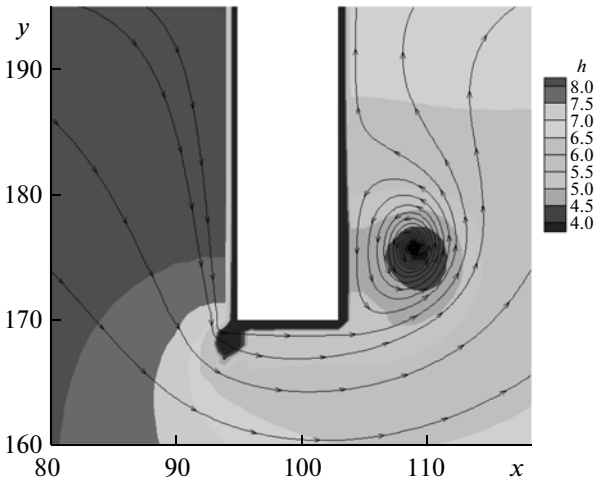

Fig. 13.

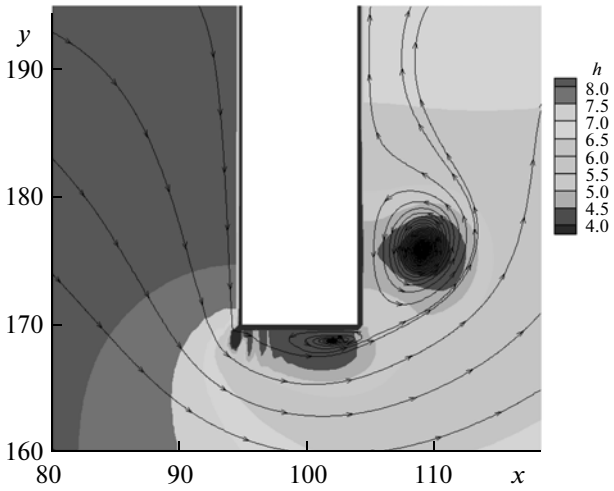

Fig. 14.

point with coordinate $x = 95$ m. Reflecting boundary conditions were set on all the boundaries of the dam; $g = 9.8$ m/s^2.

Figures 9 and 10 show the fluid height, the streamline distribution (tangents to the velocity), and lines of constant Froude number for $t = 7.2$ s computed on a uniform spatial grid with the steps $\Delta x = \Delta y = 1$ m. The computations were performed for $\alpha = 0.2$ and $\beta = 0.2$. The figure displays the characteristic features of the flow developing by the indicated time, namely, a smoothed nonmonotone profile to the left of the discontinuity, a sharp but monotone profile in the right basin, and wave reflection from the upper wall of the basin.

Figures 11 and 12 depict the one-dimensional distributions of $h(x)$ and $\mathrm{Fr}(x)$, respectively, along the line $y = 160$ m computed on a sequence of grids with the steps $\Delta x = \Delta y = 1$ (line *1*), 2 (line *2*), and 4 m (line *3*). The plots suggest that, with grid refinement, the numerical solution converges to the reference one, which was defined as the solution of the problem presented in [18]. More specifically, in [18] the dam break problem was solved on an unstructured spatial grid with the help of two high-order accurate numerical algorithms, which yielded similar results. The numerical results produced by the algorithm with regularization for $\Delta x = \Delta y = 1$ m agree well with the solution from [18] obtained with steps of ~2 m.

The two-dimensional algorithm was adapted to computations on a multiprocessor computer system with the use of geometric parallelism, MPI interface, and the C programming language. The efficiency of the parallel implementation was close to optimal, and a nearly 10 times speedup was achieved on a 10-processor system. The computations were performed on a grid with $\Delta x = \Delta y = 0.5$ m until the time $t \sim 30$ s. The resulting flow patterns show that the wave reflects from the right wall of the domain and moves back to the dam site. Additionally, a sharp increase in the fluid height is observed in the upper right corner of the right basin. The computations on a fine grid revealed the details of the formation of separated flows near the protruding segments of the dam. Specifically, more vortex formations were observed on a finer grid. Figures 13 and 14 show fragments of the vortex flow near the upper part of the dam computed on grids with steps of 1.0 and 0.5 m at the time $t = 7.2$ s. A more detailed resolution of the vortex formations can be seen on the finer grid.[1]

6. CONCLUSIONS

The QHD and QGD systems in the barotropic approximation were used to derive the SW equations with regularizers. The same equations with allowance for external forces and bed roughness were obtained using an integral representation of the SW equations. The resulting regularizing terms have the form of second spatial derivatives and are closely related to the corresponding additions to the QHD/QGD systems. The constructed additional terms do not violate the hydrostatic balance of the system.

A numerical algorithm for solving the SW equations was proposed and tested. The algorithm is based on the finite volume method with all the spatial derivatives, including the convective terms, approximated by central differences. The stability of the algorithm is ensured by the regularizing terms. The stability condition is the Courant condition.

The algorithm was tested by computing the Riemann problem, the transcritical flow over an obstacle, and asymmetric dam break. For the one-dimensional computations, the numerical results were found to converge to the analytical solutions as the spatial grid is refined. In the two-dimensional problem, the numerical results agreed with reference data obtained using high-order accurate schemes.

Due to its simplicity, accuracy, and applicability to problems of various natures, together with the low computational costs and the possibility of parallel implementation, the numerical algorithm proposed by the authors can compete with expensive high-order accurate methods.

ACKNOWLEDGMENTS

This work was supported by the Russian Foundation for Basic Research, project no. 10-01-00136.

REFERENCES

1. Yu. V. Sheretov, *Mathematical Modeling of Fluid Flows Based on Quasi-Hydrodynamic and Quasi-Gasdynamic Equations* (Tversk. Gos. Univ., Tver, 2000) [in Russian].
2. T. G. Elizarova, *Quasi-Gas Dynamic Equations* (Nauchnyi Mir, Moscow, 2007; Springer-Verlag, Berlin, 2009).
3. Yu. V. Sheretov, *Dynamics of Continuum Media under Spatiotemporal Averaging* (RKhD, Izhevsk, Moscow, 2009) [in Russian].
4. B. N. Chetverushkin, *Kinetic Schemes and Quasi-Gasdynamic System of Equations* (Maks Press, Moscow, 2004) [in Russian].
5. N. L. Sretenskii, *Theory of Wave Motions of Fluid* (Nauka, Moscow, 1977) [in Russian].
6. L. D. Landau and E. M. Lifshitz, *Fluid Mechanics* (Nauka, Moscow, 1986; Pergamon, Oxford, 1987).
7. B. L. Rozhdestvenskii and N. N. Yanenko, *Systems of Quasilinear Equations* (Nauka, Moscow, 1978) [in Russian].
8. A. G. Kulikovskii, N. V. Pogorelov, and A. Yu. Semenov, *Mathematical Aspects of Numerical Solution of Hyperbolic Systems* (Fizmatlit, Moscow, 2001; Chapman and Hall/CRC, London, 2001).
9. Yu. V. Sheretov, "On the Properties of Solutions to Quasi-Gasdynamic Equations in the Barotropic Approximation," Vestn. Tversk. Gos. Univ., Ser. Prikl. Mat., No. 3, 5–19 (2009).
10. A. A. Zlotnik and B. N. Chetverushkin, "Parabolicity of the Quasi-Gasdynamic System of Equations, Its Hyperbolic Second-Order Modification, and the Stability of Small Perturbations for Them," Comput. Math. Math. Phys. **48**, 420–446 (2008).

[1] The computations on a parallel computer system were performed by M.I. Baidasov, a student of the Faculty of Physics at Moscow State University.

11. A. A. Zlotnik, "Energy Equalities and Estimates for Barotropic Quasi-Gasdynamic and Quasi-Hydrodynamic Systems of Equations," Zh. Vychisl. Mat. Mat. Fiz. **50**, 325–337 (2010) [Comput. Math. Math. Phys. **50**, 310–321 (2010)].
12. T. G. Elizarova and M. V. Afanas'eva, "Regularized SW Equations," Vestn. Mosk. Gos. Univ., Ser. 3: Fiz. Astron., No. 1, 15–18 (2010).
13. T. G. Elizarova, M. E. Sokolova, and Yu. V. Sheretov, "Quasi-Gasdynamic Equations and Numerical Simulation of Viscous Gas Flows," Zh. Vychisl. Mat. Mat. Fiz. **45**, 545–556 (2005) [Comput. Math. Math. Phys. **45**, 524–534 (2005)].
14. Kun Xu, "A Well-Balanced Gas-Kinetic Scheme for the Shallow-Water Equations with Source Terms," J. Comput. Phys. **178**, 533–562 (2002).
15. S. Noelle, N. Pankratz, G. Puppo, and J. R. Natvig, "Well-Balanced Finite Volume Schemes of Arbitrary Order of Accuracy for Shallow Water Flows," J. Comput. Phys. **213**, 474–499 (2006).
16. A. Birman and J. Falcovitz, "Application of the GRP Scheme to Open Channel Flow Equations," J. Comput. Phys. **222**, 131–154 (2007).
17. P. Glaster, "The Efficient Prediction of Shallow Water Flows. Part II: Application," Comput. Math. Appl. **33** (9), 115–148 (1997).
18. M. Ricchiuto, R. Abgarall, and H. Deconinck, "Application of Conservative Residual Distribution Schemes to the Solution of the SW equations on Unstructured Meshes," J. Comput. Phys. **222**, 287–331 (2007).